Journal of Alloys and Compounds 514 (2012) 195–198

Contents lists available at SciVerse ScienceDirect

Journal of Alloys and Compounds

journal homepage: www.elsevier.com/locate/jallcom

# Magnetic properties and spin polarization of $Co_2Mn(Si_xSn_{1-x})$ alloys containing two $L2_1$ phases

A. Srinivasan[a,b,*], A. Rajanikanth[a], Y.K. Takahashi[a], K. Hono[a]

[a] National Institute for Materials Science, 1-2-1 Sengen, Tsukuba 305-0047, Japan
[b] Department of Physics, Indian Institute of Technology Guwahati, Guwahati 781039, India

ARTICLE INFO

*Article history:*
Received 26 September 2011
Accepted 13 November 2011
Available online 20 November 2011

*Keywords:*
Half metals
Transition metal alloys
Crystal structure
Microstructure
Magnetization
Spin polarization

ABSTRACT

Bulk $Co_2Mn(Si_xSn_{1-x})$ $(0<x<1)$ alloys have been prepared and their crystal structure, magnetization and spin polarization have been measured. X-ray diffraction pattern and scanning electron micrograph revealed the alloy phase separate into two $L2_1$ phases, $Co_2MnSi$ and $Co_2MnSn$ for $x \geq 0.25$. The saturation magnetization values corresponded to the value predicted by the Slater–Pauling (S–P) rule. Spin polarization measurements using point contact Andreev reflection (PCAR) technique showed that the quaternary alloys exhibited higher intrinsic spin polarization than the parent ternary compositions. The highest spin polarization of $0.67 \pm 0.01$ was obtained for the $Co_2Mn(Si_{0.5}Sn_{0.5})$ alloy. These studies show that isovalent substitution for Sn with Si in $Co_2MnSn$ results in enhanced intrinsic spin polarization in spite of the phase separation.



## 1. Introduction

Prediction of half-metallic behavior in NiMnSb and PtMnSb by de Groot et al. [1] has created immense interest in Heusler alloys. Subsequently, theoretical work showed that Co-based full Heusler ($X_2YZ$) alloys possess half-metallic nature [2–4]. Since an ideal half-metal exhibits 100% intrinsic spin polarization at the Fermi energy $E_F$, these materials have excellent prospect as spin injection electrodes in spintronic devices. $Co_2YZ$ alloys have received special attention due to their structural stability and high Curie temperature, which are highly desirable properties in device fabrication [5]. Achievement of giant tunneling magnetoresistance (TMR) of 570% at 2 K in $Co_2MnSi$/Al–O/$Co_2MnSi$ magnetic tunneling junction (MTJ) by Sakuraba et al. [6] has given a huge thrust to these investigations. Such a high TMR has been attributed to the half-metallic nature of $Co_2MnSi$ Heusler alloy [6]. However, the TMR value of this MTJ at room temperature was only 67%. The reason for this large temperature dependence of TMR is believed to be the presence of quasi-particle states in the spin-down density of states at $E_F$ and large decrease of the spin polarization. Fermi level tuning by alloying a fourth element to the ternary alloys has been proposed to circumvent this problem. $Co_2Cr_{1-x}Fe_xAl$ was the first alloy to be investigated on these lines [7,8]. Tezuka et al. [9] have demonstrated $E_F$ tuning in $Co_2Fe(Al_{0.5}Si_{0.5})$ alloy, which was also confirmed by our previous point contact Andreev reflection (PCAR) measurements [10]. Subsequently, several theoretical calculations have shown the possibility of tuning the density of states (DOS) of ternary Heusler alloys near $E_F$ with the addition of the fourth element and thereby obtaining half-metallic behavior [11].

The PCAR technique [12] is a simple and rapid tool for measuring the intrinsic spin polarization ($P$) of ferromagnetic materials. PCAR studies show that $P \leq 0.60$ in the ternary Heusler alloys [13–18], although TMR measurements using $Co_2MnSi$ has shown a tunneling spin polarization ($P_t$) of 0.89 [6]. We have successfully used this technique to identify several full Heusler alloys [8,17,18] with high intrinsic spin polarization such as $Co_2Fe(Ga_{0.5}Ge_{0.5})$ [19]. Current perpendicular to plane-giant magnetoresistance (CPP-GMR) device fabricated using $Co_2Fe(Ga_{0.5}Ge_{0.5})$ alloy as ferromagnetic electrodes exhibited the highest MR among Heusler alloys [20].

Spin polarization studies on the isovalent substitution of the $Z$ element in $X_2YZ$ Heusler alloys have not been reported. Though, such isovalent substitution may not modify the spin-up bands, the ensuing change in the lattice parameter is bound to influence the spin-down bands [21] and hence the spin polarization at the Fermi level. As mentioned earlier, $Co_2MnSi$, which has an $L2_1$ structure ($a = 5.64$ Å) has been shown to be half-metallic through TMR studies [6], even though PCAR experiments shows $P$ of only 0.55 for bulk $Co_2MnSi$ [15]. On the other hand, $Co_2MnSn$ ($a = 5.99$ Å and $P = 0.60$) is an intermetallic compound with strong $L2_1$ ordering [17]. In order to investigate the influence of isovalent substitution

* Corresponding author at: Indian Institute of Technology Guwahati, Department of Physics, L-Block, Guwahati, Assam 781039, India. Tel.: +91 3612582712; fax: +91 3612690762.
*E-mail address:* asrini@iitg.ernet.in (A. Srinivasan).

0925-8388/$ – see front matter © 2011 Elsevier B.V. All rights reserved.
doi:10.1016/j.jallcom.2011.11.064

for the $Z$ element in $X_2YZ$ alloys, we have prepared and studied bulk $Co_2Mn(Si_xSn_{1-x})$ alloys, and the results obtained are presented below.

## 2. Experimental

Bulk alloys with compositions of $Co_2Mn(Si_xSn_{1-x})$ ($0 < x < 1$) were prepared by melting high purity constituent elements under Ar atmosphere at a pressure of $2 \times 10^{-3}$ Pa. The as-melt alloys were sealed in silica ampoules under residual Ar pressure of $2 \times 10^{-3}$ Pa, annealed at 1100 K for 7 days and then quenched in ice water. Structural analysis of the powdered alloys was carried out with the help of a rotating anode type X-ray diffractometer (Rigaku RINT 2500) using Cu Kα X-rays. X-ray diffraction (XRD) patterns were recorded at a scan rate of 2°/min, step-size of 0.02° and tube rating of 12 kW. A scanning electron microscope (SEM, Jeol JSM-7001F) equipped with an energy dispersive spectrometer (EDS) was used to record the microstructure and estimate the composition of the crystalline phases present in the bulk samples. Magnetization measurements were performed on thin slices of samples at 10 K and 300 K with a superconducting quantum interference device (SQUID, Quantum Design MPMS2) magnetometer. Spin polarization measurements were carried out using the PCAR technique. The conductance bias voltage curves at the point contact between the superconducting Nb and the sample were measured using the lock-in technique. The normalized conductance $[G(V)/G_n]$ curves were fitted to the modified Blonder–Tinkham–Klapwijk (BTK) model [22] to deduce $P$ of the conduction electrons. A multiple parameter least squares fitting was carried out to estimate $P$ using the dimensionless interfacial scattering parameter $Z$, superconducting gap $\Delta$ and spin polarization $P$ as variable parameters.

## 3. Results and discussion

### 3.1. Structure and microstructure

Fig. 1 shows the XRD patterns of $Co_2Mn(Si_xSn_{1-x})$ ($0 < x < 1$) alloys. The intensity ($y$-axis) data has been plotted in logarithmic scale for the sake of clarity. The parent compositions $Co_2MnSn$ and $Co_2MnSi$ exhibit a single phase $L2_1$ structure with the characteristic (1 1 1), (2 0 0) superlattice reflections and the other fundamental peaks as indexed in the figure. The XRD patterns show that single phase $L2_1$ structure is retained in the $Co_2MnSn$ system with the substitution of Si for Sn up to $x = 0.3$. However, for $0.4 \leq x \leq 0.9$, each of the reflections split into doublets, indicating a dual $L2_1$ phase structure. Presence of doublets in the XRD pattern of the alloy with $x = 0.9$ indicates the negligible solubility of Sn in $Co_2MnSi$. The larger atomic size of Sn as compared to that of Si and the positive heat of mixing of these two elements are the likely reasons for this. Splitting of each $L2_1$ peak into a doublet indicates the formation of a two-phase $L2_1$ structure in $Co_2Mn(Si_xSn_{1-x})$ for $0.3 < x < 1$.

Fig. 2 shows the SEM backscattered electron images of the $Co_2Mn(Si_xSn_{1-x})$ alloys with $x = 0.25$ (or 6.25 at.%), 0.5 (or 12.5 at.%) and 0.75 (or 18.75 at.%). Fig. 2a shows that $x = 0.25$ alloy also has a two phase structure with the second phase appearing like a grain boundary phase. SEM–EDS analysis shows that the dark phase has an overall composition of $Co_{53.72}Mn_{24.44}Si_{4.80}Sn_{17.04}$ and the gray phase has an overall composition of $Co_{52.63}Mn_{25.27}Si_{3.77}Sn_{18.33}$. The variations in the composition of the two phases are in the range of 0.83–1.29 at.% which is too small to be differentiated by the X-ray diffraction technique. Hence, the phase separation in the alloys with $x < 0.3$ is not observed in the corresponding XRD patterns shown in Fig. 1. Fig. 2b shows a nearly equal distribution of the dark and gray phases in the $x = 0.5$ alloy. In this case, the dark and gray phases have compositions of $Co_{52.97}Mn_{23.99}Si_{21.46}Sn_{1.58}$ (Sn-deficient) and $Co_{48.55}Mn_{26.57}Si_{8.80}Sn_{16.08}$ (Si-deficient), respectively. The striking difference between the two phases is the Si and Sn contents. While the dark phase is Sn deficient, the gray phase is Si deficient. Fig. 2c shows the microstructure of the alloy with $x = 0.75$. A fine distribution of the two phases is seen, one enriched in Si and the other enriched in Sn. The dark and gray phases have compositions of $Co_{50.70}Mn_{25.91}Si_{22.06}Sn_{1.33}$ and $Co_{47.82}Mn_{27.08}Si_{9.12}Sn_{5.98}$, respectively. The extensive phase separation in these systems is mainly attributed to the large positive heat of mixing between Si and Sn.

### 3.2. Magnetization

Magnetization curves obtained for the $Co_2Mn(Si_xSn_{1-x})$ alloys with $x = 0.25$, 0.5 and 0.75 at 10 K are shown in Fig. 3. The samples exhibited strong ferromagnetic character by attaining magnetic

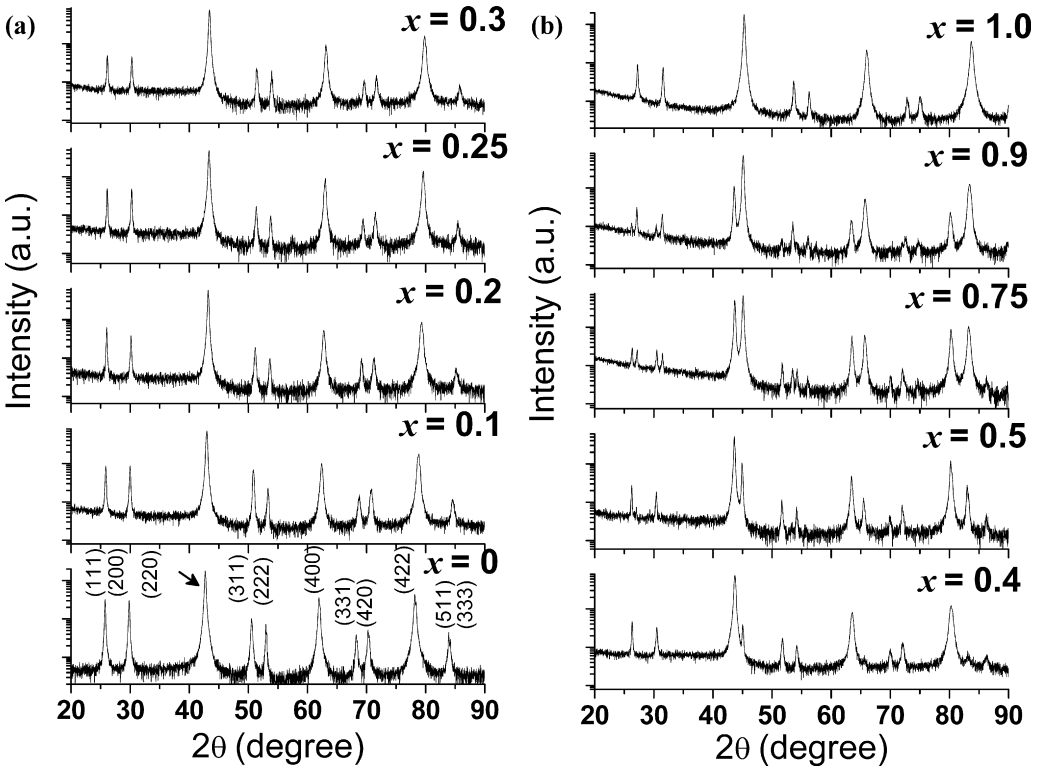


**Fig. 1.** X-ray diffraction patterns of $Co_2Mn(Si_xSn_{1-x})$ (a) ($0 \leq x \leq 0.3$) and (b) ($0.4 \leq x \leq 1.0$) alloys.

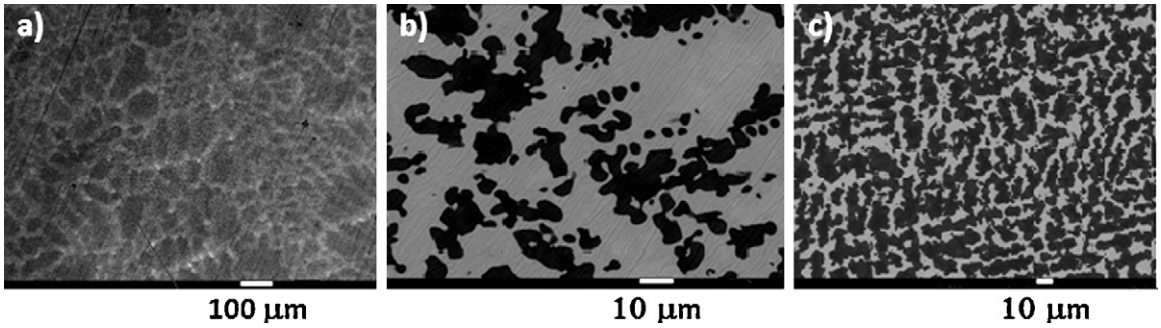


**Fig. 2.** Microstructure of (a) $Co_2Mn(Si_{0.25}Sn_{0.75})$, (b) $Co_2Mn(Si_{0.5}Sn_{0.5})$, and (c) $Co_2Mn(Si_{0.75}Sn_{0.25})$ alloys.

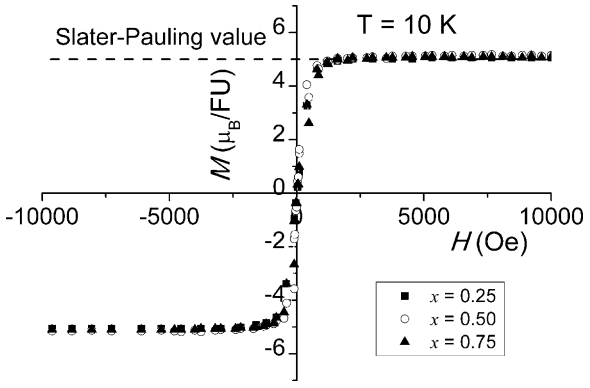


**Fig. 3.** Magnetization ($M$–$H$) curves obtained for $Co_2Mn(Si_xSn_{1-x})$ alloys with $x = 0.25$, 0.5 and 0.75 at 10 K.

saturation at relatively low fields. Total spin magnetic moment ($M_t$) predicted by the Slater–Pauling (S–P) rule [1] for $Co_2MnSi(Sn)$ is $5.0 \pm 0.1\ \mu_B$. The same can be compared with the saturation magnetization ($M_S$) obtained from the magnetization curves. $M_S$ (@10 kOe) of $x = 0.25$, 0.5 and 0.75 alloys recorded at 10 K are 5.06 ($\pm 0.05$) $\mu_B$, 5.15 ($\pm 0.04$) $\mu_B$ and 5.09 ($\pm 0.05$) $\mu_B$, respectively. $M_S$ (@10 kOe) of these alloys measured at 300 K was 4.89 ($\pm 0.05$) $\mu_B$, 5.00 ($\pm 0.03$) $\mu_B$ and 4.99 ($\pm 0.04$) $\mu_B$, respectively. It is evident that the $M_S$ values obtained for the three alloys are consistent with the $M_t$ values predicted by the S–P rule within experimental errors. The nearly temperature independent $M_S$ between 10 K and 300 K shows the strong ferromagnetic order in these alloys with Curie temperatures much higher than room temperature. This result suggests that the isoelectronic substitution of $Z$ element and the dual $L2_1$ phase structures do not affect the magnetic moments of Co and Mn.

### 3.3. Spin polarization

Fig. 4a shows the typical normalized conductance curves obtained by PCAR measurements. The data is fitted to Strijker's model [22] as mentioned earlier, to obtain the fitting variables, viz. spin polarization, $P$, interfacial scattering parameter $Z$ and superconducting band gap $\Delta$. It is possible to obtain a conductance curve corresponding to $Z = 0$ (clean interface) as shown in the case of $Co_2Mn(Si_{0.75}Sn_{0.25})$ alloy (Fig. 5b) and the $P$ estimated from such a curve corresponds to the intrinsic spin polarization. When a conductance curve corresponding to $Z = 0$ is not obtained in the PCAR experiment, the intrinsic spin polarization can be estimated by a linear fit to the $P$ versus $Z$ data and extrapolating it to $Z = 0$. Fig. 5b and c depicts the $P$ versus $Z$ plots for $Co_2Mn(Si_{0.25}Sn_{0.75})$ and $Co_2Mn(Si_{0.5}Sn_{0.5})$, respectively.

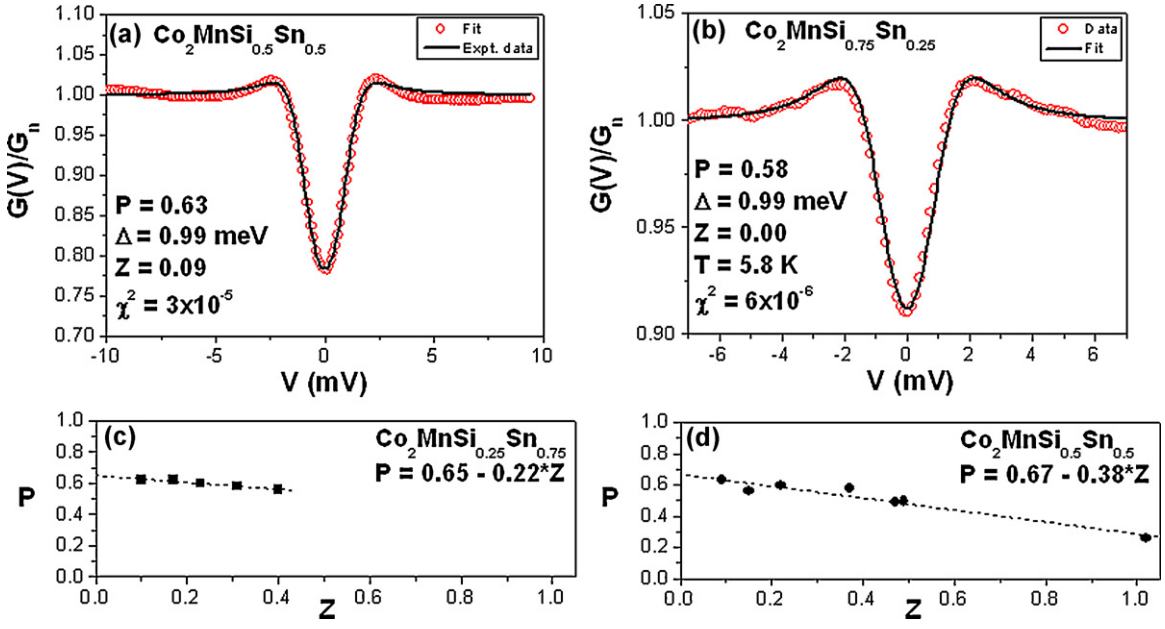


**Fig. 4.** (a) Typical PCAR conductance curves obtained for the alloys. The experimental data (open circles) has been fitted (solid line) to the BTK model and the parameters obtained are displayed. (b) The conductance curve obtained for $Co_2Mn(Si_{0.75}Sn_{0.25})$ alloy at $Z = 0$. Spin polarization versus interfacial scattering parameter $Z$ data obtained for (c) $Co_2Mn(Si_{0.25}Sn_{0.75})$ and (d) $Co_2Mn(Si_{0.5}Sn_{0.5})$ alloys have been extrapolated to $Z = 0$ for estimating the intrinsic spin polarization.

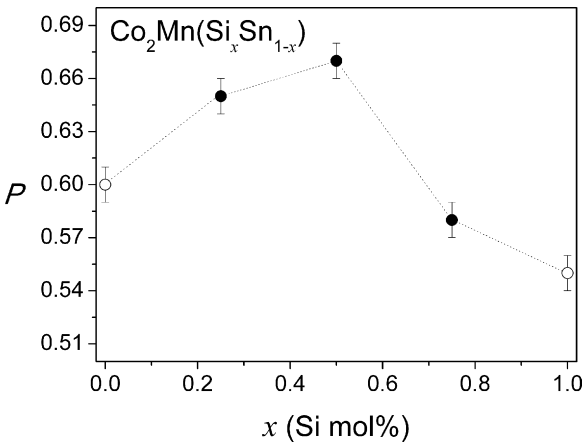


**Fig. 5.** Composition dependence of the intrinsic spin polarization ($P$) of $Co_2Mn(Si_xSn_{1-x})$ alloys. Open circles are data taken from Refs. [15,17]. Dotted line drawn merely connects adjacent data points and serves as a guide to the eyes.

$Co_2Mn(Si_{0.25}Sn_{0.75})$ and $Co_2Mn(Si_{0.5}Sn_{0.5})$ have estimated intrinsic $P$ values of $0.65 \pm 0.01$ and $0.67 \pm 0.01$, respectively.

The composition dependence of intrinsic $P$ of $Co_2Mn(Si_xSn_{1-x})$ alloys is shown in Fig. 5. Intrinsic spin polarization values estimated for $Co_2MnSi$ [15] and $Co_2MnSn$ [17] are also shown in the figure for comparison. According to the *ab initio* calculations for the DOS for $Co_2MnSn$ and $Co_2MnSi$ alloys [4,17,23], a band-gap exists in the spin-down bands for the both cases, with the center of the gap shifted towards the left and right of the Fermi level, respectively. Thus, the substitution of Sn for Sn in $Co_2MnSi$ alloy is expected to shift the Fermi level to the center of the minority electron gap. In this work, maximum spin polarization has been observed for the quaternary Heusler alloy with equal amounts of Si and Sn in accordance with this expectation. The high spin polarization for $x = 0.5$ alloy could be attributed to the high degree of $L2_1$ ordering in the dual phase alloy and the Fermi level tuning.

## 4. Conclusion

The effect of substitution of Sn with an isovalent element Si on the structure, magnetization and spin polarization of bulk $Co_2MnSn$ was investigated. $Co_2Mn(Si_xSn_{1-x})$ alloys exhibit a two-phase $L2_1$ structure due to phase separation during solidification due to the positive heat of mixing of Si and Sn. The two-phase structure does not interfere with the saturation magnetization, suggesting a strong ferromagnetic interaction between the two phases. $Co_2Mn(Si_{0.5}Sn_{0.5})$ exhibits the highest spin polarization of $0.67 \pm 0.01$, which is considerably higher than the parent ternary alloys and relatively high for Co based ferromagnetic Heusler alloys. The high spin polarization in the quaternary alloy has been attributed to the improved $L2_1$ ordering and the Fermi level tuning. The two phase alloy may provide intrinsic pinning sites for magnetic domain wall motion, thus the highly spin polarized ferromagnetic two phase alloy found in this work may lead to some unique applications in the spintronics area.

## Acknowledgements

This work was supported by the Grant-in-Aid for Scientific Research (A) 22246091. A.R. acknowledges the ICYS fellowship from the International Center for Young Scientist, NIMS.

## References

[1] R.A. de Groot, F.M. Muller, P.G. van Engen, K.H.J. Bushow, Phys. Rev. Lett. 50 (1983) 2024.
[2] S. Ishida, S. Fujii, S. Kashiwagi, S. Asano, J. Phys. Soc. Jpn. 64 (1995) 2152.
[3] S. Ishida, S. Kashiwagi, S. Fujii, S. Asano, Physica B 210 (1995) 140.
[4] I. Galanakis, P.H. Dederichs, N. Papanikolaou, Phys. Rev. B 66 (2002) 174429.
[5] B. Balke, S. Wurmehl, G.H. Fecher, C. Felser, M.C.M. Alves, F. Bernardi, J. Morais, Appl. Phys. Lett. 90 (2007) 172501.
[6] Y. Sakuraba, M. Hattori, M. Oogane, Y. Ando, H. Kato, A. Sakuma, T. Miyazaki, H. Kubota, Appl. Phys. Lett. 88 (2006) 192508.
[7] Y. Miura, K. Nagao, M. Shirai, Phys. Rev. B 69 (2004) 144413.
[8] S.V. Karthik, A. Rajanikanth, Y.K. Takahashi, T. Ohkubo, K. Hono, Appl. Phys. Lett. 89 (2006) 052505.
[9] N. Tezuka, N. Ikeda, A. Miyazaki, S. Sugimoto, M. Kikuchi, K. Inomata, Appl. Phys. Lett. 89 (2006) 112514.
[10] T.M. Nakatani, A. Rajanikanth, Z. Gercsi, Y.K. Takahashi, K. Inomata, K. Hono, J. Appl. Phys. 102 (2007) 033916.
[11] G.H. Fecher, C. Felser, J. Phys. D: Appl. Phys. 40 (2007) 1582.
[12] L. Wang, T.Y. Chen, C.L. Chien, J.G. Checkelsky, J.C. Eckert, E.D. Dahlberg, K. Umemoto, R.M. Wentzcovitch, C. Leighton, Phys. Rev. B 73 (2006) 144402.
[13] L.J. Singh, Z.H. Barber, Y. Miyoshi, Y. Bugoslavsky, W.R. Branford, L.F. Cohen, Appl. Phys. Lett. 84 (2004) 2367.
[14] M. Zhang, E. Bruck, F.R. de Boer, Z. Li, G. Wu, J. Phys. D: Appl. Phys. 37 (2004) 2049.
[15] A. Rajanikanth, Y.K. Takahashi, K. Hono, J. Appl. Phys. 101 (2007) 023901.
[16] A. Rajanikanth, D. Kande, Y.K. Takahashi, K. Hono, J. Appl. Phys. 101 (2007) 09J508.
[17] B.S.D.Ch.S. Varaprasad, A. Rajanikanth, Y.K. Takahashi, K. Hono, Acta Mater. 57 (2009) 2702.
[18] B.S.D.Ch.S. Varaprasad, A. Rajanikanth, Y.K. Takahashi, K. Hono, Appl. Phys. Exp. 3 (2010) 23002.
[19] A. Srinivasan, B.S.D.Ch.S. Varaprasad, A. Rajanikanth, Y.K. Takahashi, K. Hono, Acta Mater. (2011) communicated.
[20] Y.K. Takahashi, A. Srinivasan, B. Varaprasad, A. Rajanikanth, N. Hase, T.M. Nakatani, S. Kasai, T. Furubayashi, K. Hono, Appl. Phys. Lett. 98 (2011) 152501.
[21] I. Galanakis, J. Phys. Condens. Matter 16 (2004) 8007.
[22] G.J. Strijkers, Y. Ji, F.Y. Yang, C.L. Chien, J.M. Byers, Phys. Rev. B 63 (2001) 104510.
[23] S. Picozzi, A. Continenza, A.J. Freeman, Phys. Rev. B 66 (2002) 094421.